NATIONAL ENERGY TECHNOLOGY LABORATORY

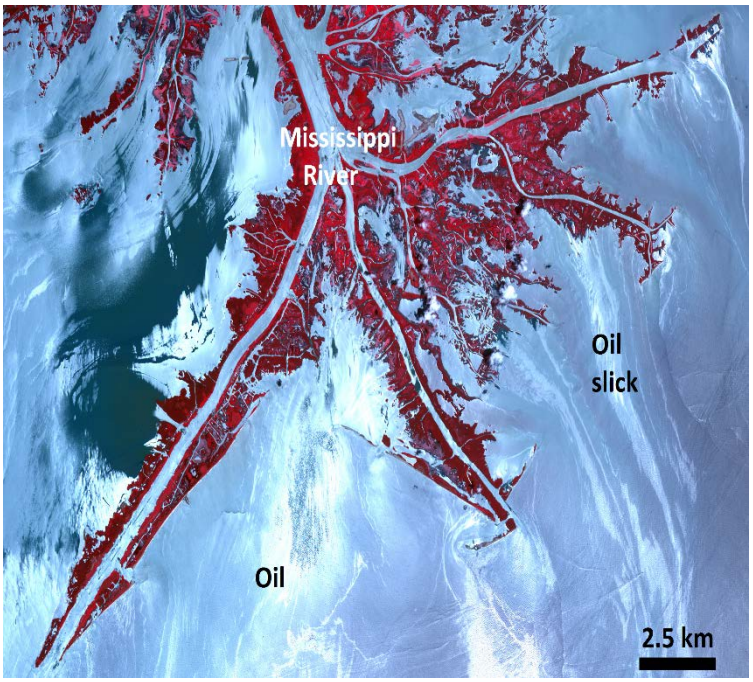

Sub-Grid Parameterizations for Oceanic Oil-Spill Simulations

28 June 2016

U.S. DEPARTMENT OF ENERGY

Office of Fossil Energy

NETL-TRS-9-2016

Disclaimer

This report was prepared as an account of work sponsored by an agency of the United States Government. Neither the United States Government nor any agency thereof, nor any of their employees, makes any warranty, express or implied, or assumes any legal liability or responsibility for the accuracy, completeness, or usefulness of any information, apparatus, product, or process disclosed, or represents that its use would not infringe privately owned rights. Reference therein to any specific commercial product, process, or service by trade name, trademark, manufacturer, or otherwise does not necessarily constitute or imply its endorsement, recommendation, or favoring by the United States Government or any agency thereof. The views and opinions of authors expressed therein do not necessarily state or reflect those of the United States Government or any agency thereof.

Cover Illustration: False-color image from NASA's Terra satellite (ASTER sensor) on May 24, 2010 showing anisotropic stirring of oil from the Deepwater Horizon as it approaches the Mississippi delta. Elongation in the direction perpendicular to the coast suggests small-scale, ageostrophic forcing. Current high-resolution operational numerical ocean models are unable to simulate such structures.

Suggested Citation: Duran, R. *Sub-Grid Parameterizations for Oceanic Oil-Spill Simulations*; NETL-TRS-9-2016; EPAct Technical Report Series; U.S. Department of Energy, National Energy Technology Laboratory: Albany, OR, 2016; p 36.

An electronic version of this report can be found at:

http://www.netl.doe.gov/research/on-site-research/publications/featured-technical-reports

https://edx.netl.doe.gov/offshore

Sub-Grid Parameterizations for Oceanic Oil-Spill Simulations

Rodrigo Duran[1,2]

[1] **U.S. Department of Energy, National Energy Technology Laboratory, 1450 Queen Avenue SW, Albany, OR 97321**

[2] **Oregon State University, 104 CEOAS Administration Building, 101 SW 26th Street, Corvallis, OR 97331**

NETL-TRS-9-2016

28 June 2016

NETL Contacts:

Rodrigo Duran, Principal Investigator

Kelly Rose, Technical Portfolio Lead

Cynthia Powell, Executive Director, Research and Innovation Center

This page intentionally left blank.

Table of Contents

EXECUTIVE SUMMARY **1**
1. INTRODUCTION. **2**
2. ADDING A "DIFFUSIVE" VELOCITY **5**
2.1 THE RANDOM WALK MODEL 5
2.2 THE RANDOM FLIGHT MODEL 6
2.3 CHOOSING THE LTS 8
2.4 THE DIFFUSION COEFFICIENT 9
2.5 THE COMBINED EFFECT OF LTS AND DIFFUSION COEFFCIENT 11
3. OTHER SEA-SURFACE PROCESSES **14**
3.1 WIND-DRIVEN CURRENTS 14
3.2 OTHER SMALL-SCALE PROCESSES 16
3.3 ON THE APPLICABILITY OF THE EKMAN-MADSEN SOLUTION AND ITS RELATION TO OTHER PHYSICAL PROCESSES 18
4. USING OBSERVATIONS INSTEAD OF OCEAN-MODELS **20**
5. OUTLOOK **22**
6. CONCLUSION. **23**
7. REFERENCES. **24**

List of Figures

Figure 1: Oil particles (black dots) after a 15-day simulation initialized on May 5, 2010 in the GoM (blue dots are the initial positions). The only velocity fields used are daily instantaneous values from HyCOM. Compare to Figure 3 where different diffusive velocities are added to the same large-scale velocity used here. Notice that without diffusion oil does not hit the coast (beached oil would show as red points as in Figure 3). 4

Figure 2: A one-dimensional stochastic path (top panel; distance in km as a function of time) resulting from the stochastic velocity (bottom panel, m/s; the mean of the stochastic velocity plus and minus a standard deviation is also shown) computed with the Langevin equation. The LTS for this one-dimensional simulation is 1 day and the period of integration is 2 days, the diffusion D is kept constant at $0.01 m^2 s^{-2}$ throughout the simulation. Notice how, in this particular example, the path changes from a positive position to a negative position when time is roughly equal to the LTS (1 day in this case). 8

Figure 3: Comparison of different diffusivity (EKE^2) and LTS combinations in open seas after a 15-day simulation ending on May 20, 2010. The large-scale velocity is daily instantaneous values from HyCOM. In each column, EKE is kept fixed to evaluate the influence of different Lagrangian time-scales. Red points show beached oil, black dots represent oil at the sea surface. 12

Figure 4: Comparison of different diffusivity (EKE^2) and LTS combinations for a semi-enclosed sea after a 2-day simulation. The large-scale velocity is daily instantaneous values from FVCOM. Red points show beached oil; black dots show oil at the sea surface. 13

List of Tables

Table 1: Angle of deflection and Ekman depth for typical summer and winter wind conditions in the Gulf of Mexico as computed with the Madsen (1977) model 15

Table 2: Angle of deflection and Ekman depth in the Salish Sea with the same wind speeds as in Table 1, computed with the Madsen (1977) model 15

Acronyms, Abbreviations, and Symbols

Term	Description
BLOSOM	Blowout and Spill Occurrence Model
DOE	U.S. Department of Energy
DWH	Deepwater Horizon
EKE	Lagrangian Eddy Kinetic Energy
GoM	Gulf of Mexico
HF	High-frequency radar
LT	Langmuir turbulence
LTS	Lagrangian Time Scale, also called Lagrangian Integral Time

Acknowledgments

This work was completed as part of National Energy Technology Laboratory (NETL) research for the U.S. Department of Energy's (DOE) Complementary Research Program under Section 999 of the Energy Policy Act of 2005. The authors wish to acknowledge Roy Long (NETL Strategic Center for Natural Gas and Oil) and Elena Melchert (DOE Office of Fossil Energy) for programmatic guidance, direction, and support.

The authors also wish to acknowledge Kelly Rose, Lawrence Sim and Tim Murin for encouragement and helpful conversations.

EXECUTIVE SUMMARY

Oil transport in the ocean is strongly determined by the effect of ocean currents. Due to limited resolution or simplifications, some components of these currents—whether derived from ocean models or observations—will likely require compensating through parameterizations for the foreseeable future. This report describes the problem and the parameterizations used as a solution, within the context of a three dimensional Blowout and Spill Occurrence Model (BLOSOM) developed by the U.S. Department of Energy (DOE). The first part of this report introduces the stochastic parameterizations implemented in BLOSOM for a small-scale diffusive velocity. The second part introduces physical processes that may need additional, deterministic parameterizations for accurate oil-spill simulations. Some sea-surface velocity products based on observations are also discussed. Recommendations for the use and future development of BLOSOM are included throughout.

1. INTRODUCTION.

Accurate ocean currents are fundamental to the success of oil-spill simulations. Numerical ocean models are often used to simulate ocean currents responding to external forcing, e.g. winds, tides, diurnal heating and cooling. However, ocean models are restricted in what they can resolve by the grid size of the numerical discretization, and the grid size is restricted (most importantly) by computing capabilities. In situ measurements of ocean currents often have similar limitations and therefore this discussion is applicable. This report uses large-scale velocity and ocean-model velocity interchangeably.

Ocean dynamics are challenging to simulate because motion at different length scales interact with each other; physical processes at scales that are not resolved are nevertheless crucial to the larger-scale solution ultimately used for oil-spill simulations. Ocean models will not be able to explicitly simulate all the scales of motion relevant to ocean dynamics in the foreseeable future. In an attempt to include the main effect of these unresolved processes, sub-grid parameterizations are often used. Likewise, sub-grid processes are a component of trajectories in the ocean, yet they are not obtainable from numerical ocean models (Kackett et al., 2006).

Representing small-scale processes and their effects in numerical ocean models will remain a fundamental, while very complicated, research area. Many of these small-scale dynamics are difficult to observe in the ocean (e.g. Moum and Rippeth, 2008), let alone understand and model them explicitly by using direct numerical simulations (in relatively small domains) and accurately parameterize them in larger-scale models (e.g. Müller and von Storch, 2004).

The scientific community is currently trying to understand the relative importance of ocean processes at different spatial and temporal scales, with an interest in both how they affect the accuracy of an ocean model solution in general, and how they would change Lagrangian trajectories in particular—both being relevant to oil-spill simulations. Understanding this is crucial because, for example, the choice of just one parameter within one parametrization, can dominate an ocean model solution (e.g. Alexandrian et al., 2012).

In general, ocean models can be calibrated to give relatively good results, and can be fairly accurate when they assimilate data to keep them from straying from observations. However, to quote the book “Ocean Modeling and Parameterization” (Chassignet and Verron, 1998):

> *The realism of large scale numerical ocean models has improved dramatically in recent years, in part because modern computers permit a more faithful representation of the differential equations by their algebraic analogs. Equally significant, if not more so, has been the improved understanding of physical processes on space and time scales smaller than those that can be represented in such models. Today, some of the most challenging issues remaining in ocean modeling are associated with parameterizing the effects of these high-frequency, small-space scale processes.*

In the presence of energetic mesoscale processes like in the Gulf of Mexico (GoM), it is often motion at the larger scales that is mainly but not completely responsible for Lagrangian motion (Beron-Vera and LaCasce, 2016; Berta et al., 2015; Liu et al., 2014; Olascoaga et al., 2013; Le Henaff et al., 2012; Beron-Vera and Olascoaga, 2009). Indeed, lateral spreading of tracers is often associated with geostrophic eddies having decorrelation times of 10 days (e.g. Ferrari and Wunsch, 2009) and large-scale motion can be considerably more energetic than the smaller-scale

(e.g. Qui et al., 2014). Motion at these larger scales is well resolved in high-resolution ocean models; however, the accuracy of that representation requires assessment.

It should be noted that when mesoscale processes are weak or moderate relative to submesocale processes, the effect of smaller-scale structures increase in importance (e.g. Shcherbina et al., 2015; Keating et al., 2011), although it is possible that even then, mesoscale motion will dominate at time scales larger than those typical for submesoscale processes (Jacobs et al., 2016). The relative importance between mesoscale and submesoscale processes as drivers of Lagrangian motion is a subject of current research, invigorated by the increasing availability of high-resolution observations and numerical ocean models.

It is assumed throughout this report that the known velocity field will be able to reproduce the strain from the large-scale structures (e.g. Poje et al., 2010). This in itself is a considerable challenge (e.g. Liu et al., 2014), but will not be discussed since it is beyond the scope of this paper.

An appropriate evaluation of the large-scale velocity is fundamental. Because what drives an oil-spill will vary and because the quality of the large-scale velocity will vary, the evaluation should be on a case-by-case basis.

The ocean-current velocity from a numerical solution could be thought of as the average over a grid cell. By averaging over an area of roughly 4 km^2, what is currently called a “high-resolution ocean model”, many of the smaller-scale horizontal processes are effectively filtered out—all ocean models are missing a small-scale “diffusive” velocity. The most common solution is to use large-scale ocean currents as an “advective velocity” and then add a “diffusive velocity” typically treated as a stochastic component (e.g. Griffa et al., 2004). The use of a stochastic component means that at best the statistical parameters of the flow can be recovered. Each simulation will be different; however, the statistics will remain the same.

Because the large-scale velocity is deterministic and often dominant, the overall patterns in which pollutions spread remain similar in different runs. However, the diffusive velocity in oil-spill modeling applications is critical for an appropriate spreading of the oil and for beaching to occur. Trajectories from the large-scale velocity field do not reach the coast due to the boundary conditions imposed on the velocity during the model’s integration: because water cannot cross a solid boundary, the velocity normal to the boundary is set to zero at the boundary or nearby (see e.g. the introductory discussion in Samelson, 1997). Thus, it is the diffusive velocity that allows oil to hit the coast.

Resolution in the vertical coordinate is also limited in ocean models so that turbulence models (i.e. one-dimensional parameterizations of vertical fluxes) are critical. In the ocean, vertical length-scales are considerably smaller than horizontal length-scales; thus, due to insufficient vertical resolution, even currents that ocean models can simulate fairly well (e.g. Ekman velocity; Durski et al., 2004, Large et al. 1994) may be missing or underrepresented. In this case, an oil-spill model will need to add an Ekman velocity computed directly from wind data. This option is also useful when the large-scale velocity includes only tides, or altimetry.

A further potential complication is that ocean models do not typically output solutions for some of the physical processes that may affect trajectories in the ocean (e.g. waves, windage are missing; Hackett et al., 2006; Wu et al., 2015). Whenever these absent processes are relevant, an

ad hoc way to alleviate their absence is to likewise parametrize them and add the resulting small-scale velocity to the large-scale velocity.

An alternative to these parameterizations is to use observations: it is possible to measure a wider spectrum of currents responsible for Lagrangian transport directly at sea. From that information, it may be possible to compute trajectories directly; alternatively, it may complement large-scale motion from other sources with small-scale processes. Caveats from these methods are discussed below.

The limitations described above affect BLOSOM (Blowout and Spill Occurrence Model), a three-dimensional blowout and oil-spill model (Sim et al., 2015), just as it would affect any oceanic oil-spill model. This report describes some of the methods BLOSOM uses to alleviate the problem, including recommendations on how the parametrizations can be used. The first part of this paper discusses how to add a "diffusive" velocity and the second part, how to include missing physics that may be needed to accurately simulate trajectories of passive objects in the ocean. Methods that may be implemented in the future and their rational are also suggested.

These examples show that, depending on the objectives, physical oceanographers should be involved in the different aspects of the prediction of Lagrangian trajectories, from acquiring an adequate ocean current velocity (which may require finding an adequate ocean model or otherwise) to assessing the results and any potential need for improvement.

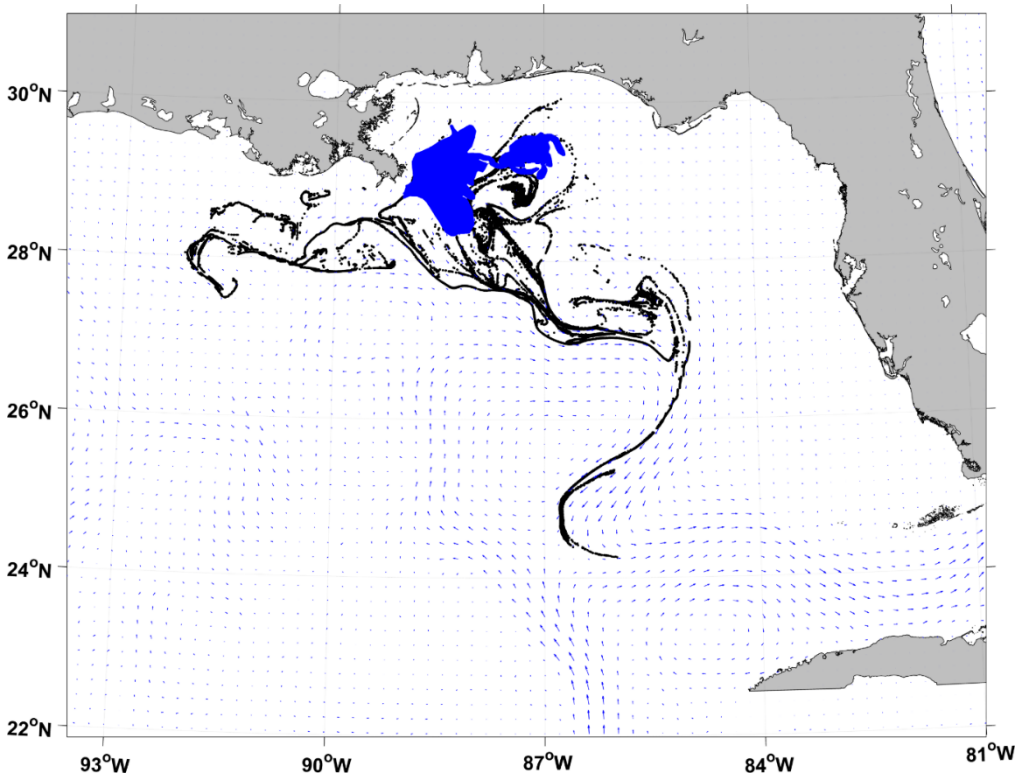

Figure 1: Oil particles (black dots) after a 15-day simulation initialized on May 5, 2010 in the GoM (blue dots are the initial positions). The only velocity fields used are daily instantaneous values from HyCOM. Compare to Figure 3 where different diffusive velocities are added to the same large-scale velocity used here. Notice that without diffusion oil does not hit the coast (beached oil would show as red points as in Figure 3).

2. ADDING A "DIFFUSIVE" VELOCITY

BLOSOM offers two options for computing a diffusive velocity: a random walk and a random flight. The methods are called zero and first-order Lagrangian Stochastic models, respectively. This section describes the methods, the user-defined parameters, and some general guidelines on how to choose these parameters. Further discussion on these topics can be found in Fischer et al. (1979), Heemink (1990), Rupolo (2007a, 2007b), LaCasce (2008), and Haza et al. (2012).

A problem with both of these models is that they assume homogenous and stationary turbulent flow. Berloff and McWilliams (2002) offer correction terms that could be added.

2.1 THE RANDOM WALK MODEL

This method was proposed by Albert Einstein to simulate molecular diffusion by computing the statistics of molecule motion. Due to the extremely large number of molecules in any small volume (e.g. there are ~ 10^{26} molecules of water in a cubic centimeter of water) it is natural to assume that because molecules collide extremely frequently, they would quickly lose the influence of its previous velocity; the result is a random path. This method is analogous to the diffusion equation (Fischer et al., 1979) and therefore, may simulate the statistics of turbulent motion at scales larger than molecules.

To simulate diffusion, a random position increment is scaled with a random number from a Gaussian distribution $\mathbf{N}(t)$ with zero mean and a variance of one as follows:

$$d\mathbf{x} = (2\mathbf{K}dt)^{\frac{1}{2}}\,\mathbf{N}(t)$$

The diffusion coefficient **K** is discussed below.

Using a different probability distribution would give accurate results only after several small time-steps, i.e. until there is convergence to a Gaussian distribution under the central limit theorem. This would unnecessarily increase the minimum resolved time scale—see Hunter at al. (1993) for the details including the conditions for using a distribution other than Gaussian.

When using vast amounts of random numbers, the suitability of the number generator should be a concern, a simple test is outlined in Hunter at al. (1993).

The stochastic increment $d\mathbf{x}$ is added directly to the ocean-model trajectory increment $d\mathbf{X}$ (Berloff and McWilliams, 2002; LaCasce, 2008):

$$d\mathbf{X} + d\mathbf{x} = \mathbf{U}dt + (2\mathbf{K}dt)^{\frac{1}{2}}\,\mathbf{N}(t)$$

Where $\mathbf{U}dt$ represents any type of time-integration scheme for the large-scale velocity.

Accordingly, probability distribution P for a particle's position is governed by the Fokker-Plank equation

$$\frac{\partial P}{\partial t} + \mathbf{U} \cdot \nabla P = \nabla(\mathbf{k} \nabla P)$$

for which the solution is a Gaussian distribution. Note that this equation is analogous to the diffusion-advection equation, but uses an eddy diffusivity coefficient **k** instead of molecular diffusivity.

Implicit assumptions in the random-walk model is that the mean (or large-scale) and diffusive velocities can be efficiently separated, however this assumption is problematic (De Dominicis et al., 2012). Undesirable consequences of this assumption are that the diffusive velocity is never autocorrelated and that spreading is always linear without quadratic growth at initial times (e.g. LaCasce, 2008). Further discussion on the applicability of the diffusion-advection equation can be found in De Dominicis et al. (2012) and references therein.

2.2 THE RANDOM FLIGHT MODEL

The random flight model assumes instead that the diffusive velocity is partly random, but also has some memory. It is natural to consider a method with memory since the physical processes (e.g. small-scale coherent structures) being parametrized are unlikely to influence a trajectory only for an instant. The Lagrangian velocity from drifters in the ocean remains significantly autocorrelated for a period of time that varies according to both local and remote ambient conditions.

In this model, it is the diffusive velocity that is simulated instead of directly simulating the diffusive trajectory. Consider the differential equation governing each component of a three-dimensional trajectory in the ocean, with a deterministic component $\mathbf{X} = \mathbf{X}(t)$ and a stochastic component $\mathbf{x} = \mathbf{x}(t)$:

$$\frac{\mathrm{d}\mathbf{X}}{\mathrm{d}t} + \frac{\mathrm{d}\mathbf{x}}{\mathrm{d}t} = \mathbf{U} + \mathbf{u}$$

Where **U** is the large-scale, advective velocity and **u** is the diffusive velocity. This differential equation is a linear combination of an ordinary and a stochastic differential equation. The Langevin equation governs the evolution of the diffusive velocity:

$$\mathrm{d}\mathbf{u} = -\frac{\mathbf{u}}{T_L}\mathrm{d}t + D\mathrm{d}\mathbf{W}_t$$

where $\mathrm{d}\mathbf{W}_t$ is an infinitesimal increment of a Wiener process which is temporally uncorrelated, normally distributed with zero mean and variance $\mathrm{d}t$. This equation requires choosing two parameters: relaxation time T_L and a diffusion coefficient D; both are discussed further below.

(The suitability of the random number generator mentioned in the section above also applies here.)

When the Langevin equation is used to compute a diffusive velocity increment, heuristic insight can be gained from the equation:

$$\mathbf{u}(t+dt) = \mathbf{u}(t) + d\mathbf{u} = \mathbf{u}(t)\left(1 - \frac{\mathrm{d}t}{T_L}\right) + D\mathrm{d}\mathbf{W}_t$$

A large relaxation time T_L relative to dt, makes the term $\left(1 - \frac{\mathrm{d}t}{T_L}\right)$ slightly smaller than one, so that the new stochastic velocity $\mathbf{u}(t+dt)$ is similar but slightly smaller in magnitude than $\mathbf{u}(t)$. (Note that if there is a different relaxation time for each component of the diffusive velocity, then the direction will also change.) This is the case when the diffusive velocity has a strong memory.

When the elapsed time equals the relaxation time (say for $\mathrm{d}t = T_L$ above), the new stochastic velocity is completely random and therefore it is uncorrelated with the previous one.

Thus, the period of time during which the process retains a memory is the Lagrangian Time Scale (LTS; also called Lagrangian Integral Time), defined as:

$$T_L \equiv \int_0^\infty R(\tau)d\tau$$

Here, $R(\tau)$is the Lagrangian-velocity autocorrelation function. In practice, the first lag-time at which $R(\tau)$ crosses zero is often used to compute LTS from observations.

The random flight model requires an Ito integral of the Langevin equation (the integral is called "Ornstein-Uhlenbeck process") to get the time-dependent stochastic velocity **u**, a second Ito integral gives $\mathbf{x}(t)$, the stochastic trajectory. BLOSOM uses exact numerical formulas for both of these stochastic integrals (Gillespie, 1996), also used for the simulations in this paper. Thus, this model forces **u** to be consistent with observations by remaining autcorrelated for a period equal to LTS (Figure 2).

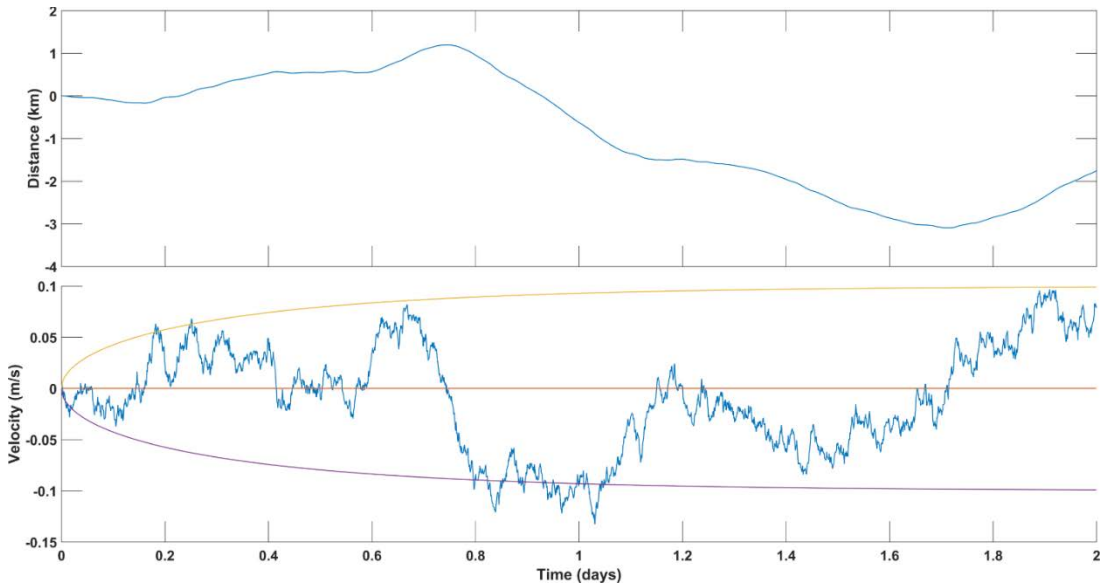

Figure 2: A one-dimensional stochastic path (top panel; distance in km as a function of time) resulting from the stochastic velocity (bottom panel, m/s; the mean of the stochastic velocity plus and minus a standard deviation is also shown) computed with the Langevin equation. The LTS for this one-dimensional simulation is 1 day and the period of integration is 2 days, the diffusion D is kept constant at 0.01m^{2}s^{-2} throughout the simulation. Notice how, in this particular example, the path changes from a positive position to a negative position when time is roughly equal to the LTS (1 day in this case).

The Ornstein-Uhlenbeck process captures two properties expected from dispersion under the assumption of stationary flow: 1) at first ($t \ll T_L$) dispersion increases quadratically in time, and 2) at long times ($t \gg T_L$) it increases linearly (LaCasce, 2008).

This process also satisfies a Fokker-Plank equation although a more complicated one than in the random walk case (e.g. LaCasce, 2008.)

There are two parameters needed for the random flight model, the LTS and the diffusion coefficient, which are discussed in the following sections.

2.3 CHOOSING THE LTS

A typical value for LTS at the sea surface (which is more energetic) is a few days, it increases to about 3–8 days at depths between 400–1,000 m where motion is less energetic. Lumpkin et al (2002) and Rupolo (2007b) show global maps of LTS computed from observations, they may be used as a first guess when using BLOSOM. Analytical relations between the Eulerian and Lagrangian time scales have been researched, if appropriate Eulerian data is available these relations can be used to find an appropriate LTS (Middleton, 1985; Lumpkin et al., 2002; Chiswell, 2013; see Section 2.8 of LaCasce, 2008). Ideally one would have ocean data for the region and time (or season) of interest with which the Lagrangian time scale can be computed. Realistically, this information may not always be attainable, although global data is becoming increasingly available (e.g. http://www.aoml.noaa.gov/phod/loopers/).

Another caveat is that the LTS varies with depth (e.g. Chiswell 2013). BLOSOM is a three-dimensional blowout model simulating oil droplets rising through the water column as ocean

currents disperse them. A simple solution to the TLS depth-dependence is to use one LTS value at depth and another one near the surface (e.g. above the maximum buoyancy frequency). Some preliminary testing has been conducted, but a vertical dependence has not been implemented in the current release. It is recommended that a future version does include the capability of using two LTS values; this is especially important for blowouts where oil remained at depth for relatively long periods of time (e.g. McNutt et al., 2012; Valentine et al., 2014).

2.4 THE DIFFUSION COEFFICIENT

Sub-grid has different meanings depending on the ocean-model's resolution. It is important to consider the sub-grid parameterization, the ocean-model's resolution and the interaction between these two factors in order to simulate Lagrangian statistics (e.g. dispersion) appropriately (see e.g. Haza et al., 2012; Zhong and Bracco, 2013). Sub-grid parameterizations should improve the statistics in simulated trajectories by approximating dispersion due to missing mesoscale or submesoscale dynamics (see e.g. Lacorata et al., 2014 or Haza et al., 2012, respectively). Thus, a desirable property is that the diffusion coefficient be able to account for the ocean-model's resolution without user intervention. A Smagorinsky diffusivity (Smagorinsky, 1993) coefficient increases when resolution is coarser or when the velocity strain increases:

$$D_{\mathrm{SMAG}} = k\,\Delta x \Delta y \sqrt{\left(\frac{\partial u}{\partial x}\right)^2 + \frac{1}{2}\left(\frac{\partial u}{\partial y} + \frac{\partial v}{\partial x}\right)^2 + \left(\frac{\partial u}{\partial x}\right)^2}$$

BLOSOM uses this definition for diffusivity with a default constant k=0.15, (it is user adjustable). It effectively uses the grid size Δx or Δy as the length-scale for unresolved turbulence and Δu or Δv as the scale for the turbulent velocity (e.g. Section 1.4 of Tennekes and Lumley, 1972). However, despite its popularity, defining a diffusion coefficient by using a "mixing" length scale and a turbulent-velocity has some shortcomings (e.g. mixing-length model in Section 2 of Tennekes and Lumley, 1972, see also Large et al., 1994).

There are other properties for which this diffusion coefficient is not as popular with tracers. (It is more commonly used for momentum; the implicit assumption in Smagorisnky's formulation is that the Prandtl number is equal to one; tracer diffusivity and momentum viscosity are equal.) Of interest to this application is that strain is often large near the boundaries, causing unrealistic mixing—this is known as the Veronis effect (e.g. Veronis, 1975). In the context of oil-spills, this could mean excess beaching.

Finally, it can be shown that the random walk model with a spatially varying diffusion coefficient, as defined above, causes an error equivalent to the omission of an "apparent advection velocity, in the direction of increasing diffusivity and of magnitude equal to diffusivity gradient" (Hunter et al., 1993, see also Cushman-Roisin and Beckers, 2011). This problem causes agglomeration of particles in regions of small diffusivity; it can be especially problematic when large-scale currents are small. In the context of ocean oil-spills, for example, this could happen during a deep blowout enclosed within—and therefore shielded by—a deep and relatively small basin.

Other disadvantages of this method are common to other diffusion coefficients and therefore discussed below.

Further discussion on Smagorisnky diffusivity can be found in Griffies (2004, e.g. Section 18).

BLOSOM offers an alternative diffusion scheme, a first-order stochastic model named "random flight". The diffusion coefficient for the first-order LSM is based on the Lagrangian Eddy Kinetic Energy (EKE) defined in Rupolo (2007b) as:

$$D_{EKE} = \sqrt{\frac{2\sigma^2}{T_L}}$$

Where $\sigma^2 = \frac{1}{2}(\sigma_u^2 + \sigma_v^2)$, and the zonal EKE is $\sigma_u^2 = \frac{1}{N-1}\sum_{n=1}^{N}(u_n - \bar{u})^2$ with $\bar{u} = \frac{1}{N}\sum_{n=1}^{N} u_n$. This is a Lagrangian definition: u_n is the velocity between points x_n and $x_{n+1}$of a particle's trajectory. A similar expression is used for the meridional EKE σ_v^2. This definition is motivated by an observed relationship between horizontal diffusivity and EKE, it seems a particular good approximation when computed from observations (Bauer et al., 2002; Rupolo, 2007a; De Dominicis et al., 2012). Defining the EKE-based diffusivity using the ocean-model velocity is problematic because:

1. As resolution increases, submesoscale motion becomes explicitly simulated reducing the need for parametrization, yet, EKE increases with increased resolution; the result is that D_{EKE} increases in magnitude when a smaller diffusion coefficient is needed. For example: a 1.5 km resolution ocean-model solution showed a ten-fold increase in eddies and EKE when compared to a 15-km resolution solution (Klein and Lapeyre, 2009 and references therein).
2. EKE from mesoscale and submesoscale motion have different annual cycles (e.g. Qiu et al., 2014, Callies et al., 2015). Thus, an accurate mesoscale ocean-model should not be expected to produce an EKE-based diffusion coefficient that accurately parametrizes the missing submesoscale motion, even if there was a way to scale the magnitude of the diffusion coefficient to solve the problem mentioned in point 1.

Other concerns include:

1. The definition of EKE involves subtracting a temporal mean ($\bar{u}$) that is often difficult to define objectively and consistently (e.g. Bauer et al., 2002; De Dominicis et al., 2012).
2. Both formulations for eddy diffusivity above are isotropic. Anisotropy tends to be important due to vorticity conservation (both topographic and planetary, e.g. Bauer et al., 2002) and also because mixing is often an order of magnitude greater along the mean flow than across it (e.g. Maurizi et al., 2004, De Dominicis, 2012); indeed, anisotropy may help alleviate the Veronis effect (e.g. Gent, 2011). A related problem with the random flight method is that the LTS should be greater in the direction of the mean flow than in the cross direction e.g. Maurizi et al. (2004), De Dominicis (2012).

3. Recent observations near the Deep Horizon blowout suggest the irregular bathymetry over the northern GoM may be an important feature to account for in dispersion studies because it increases diffusivity (Ledwell et al., 2016). This is another reason why it is desirable for a diffusion scheme to keep tracers over the slope in a realistic manner (related to previous point).

Despite receiving considerable attention, parametrizing an accurate diffusion coefficient is still an open problem in oceanography. Thus, measuring it directly from observations seems a natural strategy, although still under development (e.g. De Dominicis et al., 2012). This approach is often limited to the sea surface, and further, it does not solve the need for an accurate large-scale velocity. Computing an eddy diffusivity from satellite observations (Sallée, 2008) has similar disadvantages; furthermore, it may need region-dependent calibration. Techniques using observations that are more comprehensive are discussed in the Section 4, below.

A viable and recommended option is then to use a tracer eddy diffusivity as outputted from the ocean model—often a readily available quantity. Ocean models use sophisticated parametrizations that tend to alleviate the problems mentioned above. The eddy diffusivity from an ocean model D can be used directly for the random walk model; but for the random flight model the relation $D \approx \sigma^2\, t$ that holds for $t \ll T_L$ (e.g. Thorpe, 2007) is used to compute $\sigma^2 \approx \frac{D}{\Delta t}$ (here Δt is BLOSOM's time step), from where:

$$D_{EKE} = \sqrt{\frac{2D}{\Delta t\, T_L}}$$

2.5 THE COMBINED EFFECT OF LTS AND DIFFUSION COEFFCIENT

The following experiments highlight the influence of the user-dependent parameters in the Langevin equation. These simulations use nearest-neighbor interpolation to avoid introducing sub-grid variability when interpolating the large-scale velocity (even though it may not make a noticeable difference).

Sensitivity tests suggest that changing the value of LTS is less influential than changing the value of the diffusion coefficient D. Further testing, however, also suggests that the LTS value may be of greater importance in enclosed or semi-enclosed seas.

When the coast is not necessarily close by, a larger LTS will cause greater spread. Loosely speaking, the diffusive (random) trajectory for each particle is able to stay its course for a longer time, travelling further (see the discussion on Langevin equation above). However, the diffusion has a greater influence on the spread, as compared to the influence due to LTS. For example, an eightfold increase in LTS is similar to a threefold increase in D (Figure 3). In this example, a threefold increase in D may produce increased beachings in the Northern GoM and even in Cuba, while a threefold increase in LTS only produces a relatively small increase in beaching in Northern GoM.

The relative importance of the diffusion coefficient in small enclosed or semi-enclosed seas (i.e. when the coast is always relatively close) is somewhat reduced. When land is nearby trajectories are more likely to miss the entrance of a small bay or inlet if they have less freedom to change direction. A shorter LTS allows the trajectory to change direction more often, increasing the chances of entering a small enclosure or bay. Thus, a short LTS increases spreading and more coastline is impacted, while a longer LTS causes particles to beach nearby as they stay their course (Figure 4).

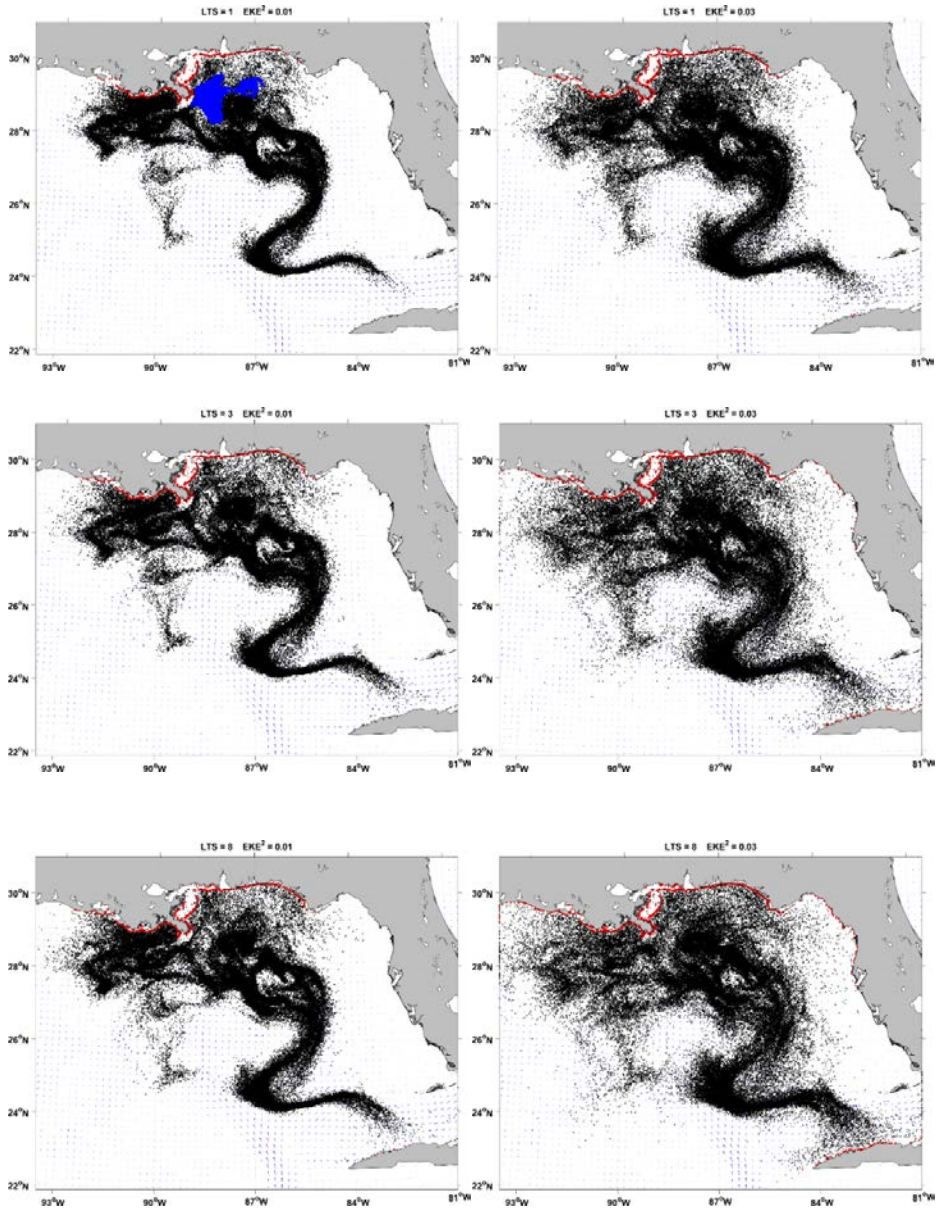

Figure 3: Comparison of different diffusivity (EKE^2) and LTS combinations in open seas after a 15-day simulation ending on May 20, 2010. The large-scale velocity is daily instantaneous values from HyCOM. In each column, EKE is kept fixed to evaluate the influence of different Lagrangian time-scales. Red points show beached oil, black dots represent oil at the sea surface.

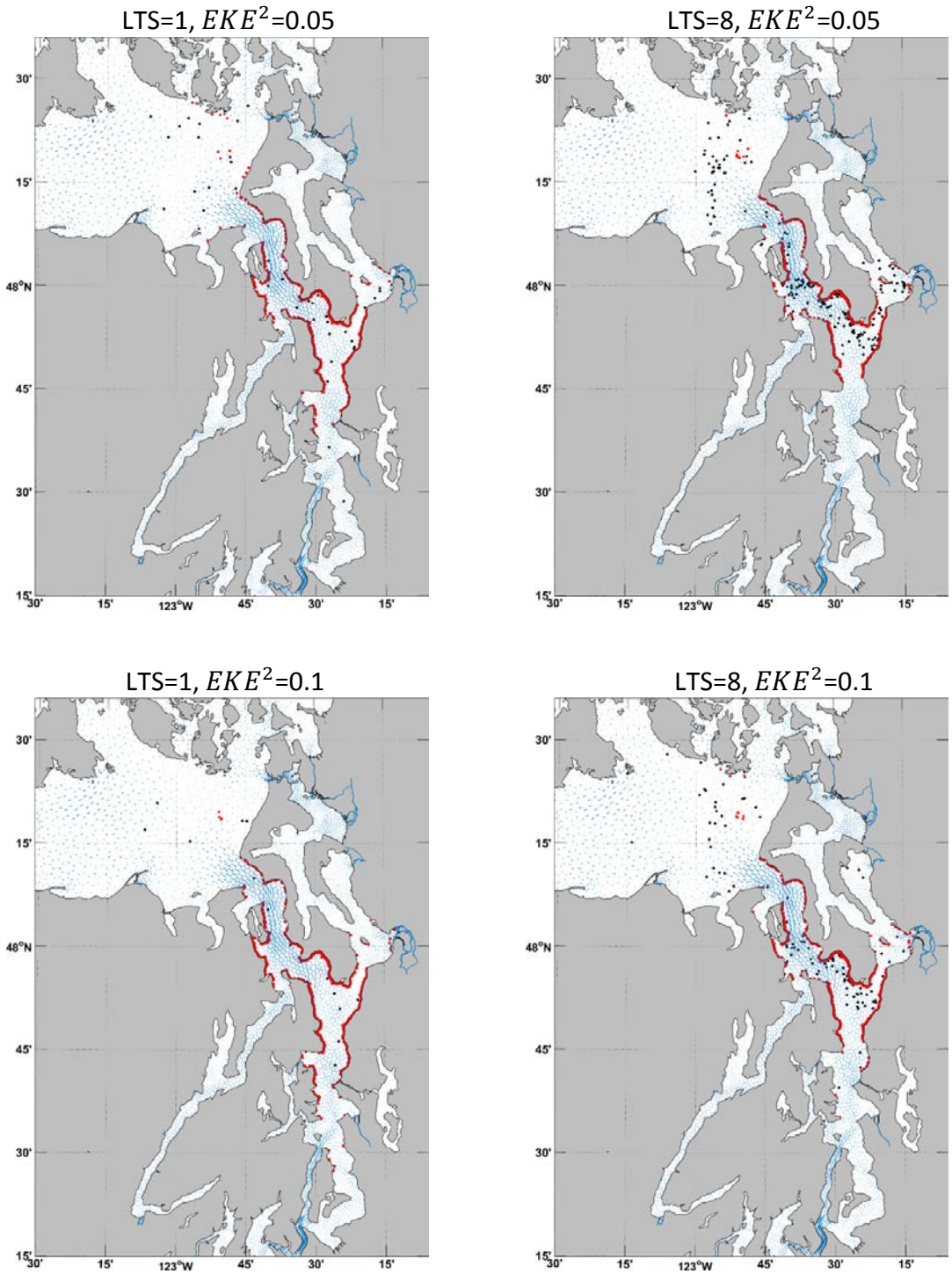

Figure 4: Comparison of different diffusivity (EKE^2) and LTS combinations for a semi-enclosed sea after a 2-day simulation. The large-scale velocity is daily instantaneous values from FVCOM. Red points show beached oil; black dots show oil at the sea surface.

3. OTHER SEA-SURFACE PROCESSES

This section describes physical processes that may be incomplete or absent in ocean model solutions but that may be important when simulating trajectories; some discussion on how to include their effects and recommendations for future BLOSOM development is included. The use of sea-surface velocity products that combine different measurements of the ocean is also briefly discussed as an alternative to using ocean models.

3.1 WIND-DRIVEN CURRENTS

The effect of wind on the ocean's surface is an important problem originally solved by Ekman (published in 1905). The most famous result of his work is the analytical expression for a steady, frictional velocity on a rotating planet, a solution to the equation that relates the ageostrophic Coriolis acceleration to turbulent diffusion of momentum:

$$f\,\hat{\mathbf{n}} \times \mathbf{u_E} = \frac{\partial}{\partial z}\left(K_m \frac{\partial}{\partial z}\mathbf{u_E}\right)$$

Here $\hat{\mathbf{n}}$ is the vertical unit vector. The Ekman velocity $\mathbf{u_E}$ that solves the above equation changes in magnitude and direction with depth (the famous Ekman spiral) and represents a basic solution for wind forcing through turbulent transfer of momentum into the ocean. The solution is valid over a vertical lengthscale called Ekman layer depth that is obtained directly from the solution.

The original formulation of the problem assumes that the eddy diffusivity K_m is a constant. In the ocean, however, it has temporal, vertical, and horizontal variability. A more realistic representation of the boundary layer in the Ekman problem is due to Madsen (1977), which assumed vertical variation of K_m. The eddy diffusivity is simulated as a linear function resulting in the realistic effect of allowing bigger eddies as depth increases. A consequence is that in the Madsen solution, the Ekman velocity deflects less: at the surface it is now directed to about 10° to the right of the wind direction (to the left in southern hemisphere) instead of 45° in the classical Ekman solution. The rest of the spiral also has less deflection.

In Madsen's formulation, the exact angle of deflection at the surface depends on the strength of the wind and the latitude. It can be computed (in radians) with the following formula (Equation 39 in Madsen, 1977):

$$\phi_s = \operatorname{atan}\frac{\frac{\pi}{2}}{-1.15 + \ln\frac{30\,d}{k_s}}$$

Here $k_s \approx 0.05\,m$ is an estimate for sea surface roughness (the solution is not very sensitive to this quantity so using the provided value is adequate), and $d \approx \frac{3.66W_{10}}{\sin\theta}$ is the vertical length

scale that determines the depth of frictional wind influence (i.e. the Ekman layer depth). W_{10} is the speed of wind 10-m above the ocean's surface in meters per second (m/s) and θ is the latitude in radians. Typical values in the GoM for the Ekman-layer depth and angle of deflection for the wind-driven ocean current at the surface as computed from the Madsen model are given in the following table:

Table 1: Angle of deflection and Ekman depth for typical summer and winter wind conditions in the Gulf of Mexico as computed with the Madsen (1977) model

Latitude	Summer Wind Speed	Winter Wind Speed
	$W_{10} = 4\,m/s$	$W_{10} = 9\,m/s$
Southern GoM, $\theta = 18N$	$d = 35m;\ \phi_s = 10.1°$	$d = 106m;\ \phi_s = 9°$
Northern GoM, $\theta = 30N$	$d = 22m;\ \phi_s = 10.7°$	$d = 65m;\ \phi_s = 9.5°$

These wind speeds are representative of climatological summer and winter conditions in central GoM (winds are generally weaker during the summer). Interestingly, the Ekman layer depths as computed above are similar to the climatological mixed layer depths reported in Muller-Karger et. al. (2015) for summer and winter. Mixed-layer depth and Ekman depth are not necessarily the same—e.g. up to 50% of coastal-upwelling Ekman transport can happen below the surface mixed layer (Lentz, 1992).

An example with the same wind speeds as above, but at a latitude $\theta = 47.75N$ that is representative of the Salish Sea gives:

Table 2: Angle of deflection and Ekman depth in the Salish Sea with the same wind speeds as in Table 1, computed with the Madsen (1977) model

Summer Wind Speed	Winter Wind Speed
$W_{10} = 4\,m/s$	$W_{10} = 9\,m/s$
$d = 20m;\ \phi_s = 10.8°$	$d = 45m;\ \phi_s = 9.9°$

In the Madsen model (1977), and when the effect of wind acting on an oil slick is neglected (instead of directly on the ocean's surface), the magnitude of the Ekman velocity at the surface is about 2.5–3.6% of W_{10} (computed with values from Table 1 in Madsen, 1977). Note that this velocity does not include geostrophic contributions.

If the time-dependent problem is solved, a spin-up time from the Madsen model can be computed as a function of the inertial period which in turn depends on the latitude. In the GoM for example, the ocean's response to wind in the Ekman layer will reach a steady state in about 8 hrs (northern GoM) to 12 hrs (southern GoM). At a latitude representative of the Salish Sea, say

47.7N, steady state is reached in about 5 hrs. The hope is that a steady state will be an adequate approximation, indeed most of the energy from winds forcing currents is at periods of a few to several days. The validity of this assumption may need verification in certain locations.

In the steady state, the angle of deflection between the ocean current and the wind increases with depth, and the magnitude of the ocean current decreases rapidly. If the surface-current deflection is about 9° to the right (to the left in the southern hemisphere) of W_{10}, then at a depth equal to 1% of the Ekman layer depth *d*, the angle is about 25°, and the speed of the ocean current decreases to about 1⁄3 of the ocean-current speed at the surface. One percent of the Ekman layer depth d in the examples in the tables above is between 20 cm to 1 m. At a depth equal to 4% the Ekman layer depth, the angle is 33° and the speed is about 1⁄4 of the surface current speed. That would be at a depth between 0.8 to 4 m in the examples above.

A result that is similar to this Madsen model can be derived by simply adding a “law of the wall” defect velocity at the surface to the classical Ekman solution (e.g. Csanady, 1982). This approach results in an angle of deflection of about 20° at the surface, which also often agrees well with observations.

3.2 OTHER SMALL-SCALE PROCESSES

There are other small-scale processes not typically represented in ocean models that are able to influence the advection of particles. For example the nonlinear effects of inviscid waves: Stokes drift and waves breaking and adding momentum to the surface currents (see e.g. Kraus and Businger, 1994; McWilliams and Restrepo, 1999; McWilliams et al., 2012; Wu et al., 2015); or Langmuir turbulence (LT) which is one of the key nonlinear vertical mixing processes at the sea surface (Skyllingstad et al., 1996). LT is due to the combined effect of surface waves and wind (Moum and Smyth, 2001). Nonbreaking waves also stir the sea-surface enhancing mixing and oil emulsification. To quote a recent review on turbulence in the upper-ocean by D'Asaro (2014):

> *Observations now show that the upper-ocean boundary layer differs fundamentally from the classical laboratory and atmospheric boundary layer owing to the influence of surface waves. The differences appear in at least two ways. First, wave breaking produces a layer of intense turbulence near the surface, with dissipation rates much higher than those in the classical model. This has been known for many years and continues to be verified. Second, and more recently, measurements below the wave-breaking layer show significant deviations from the classical model in the form of the turbulence, consistent with the predictions of LES models of Langmuir turbulence driven by the Stokes drift of the waves. The resulting turbulent eddies are more coherent, have a larger vertical velocity, and mix more effectively. … Thus, although the existing observations support the hypothesis that Langmuir turbulence—driven by air–sea fluxes of momentum, heat, and moisture and the profile of surface wave Stokes drift, and modified by surface wave breaking—describes the upper-ocean boundary layer, the data available are very limited, especially from the open ocean. In particular, we do not know when, where, or how Langmuir turbulence becomes a poor representation of the boundary-layer turbulence.*

Clark (2015) estimated Stokes drift during the DWH event (April–July 2010) to be for the most part between 1–4 km/day and reaching up to about 8 km/day. Hurricane Alex in (late June–early

July 2010) skewed the distribution of Stokes-drift velocity towards higher values: during the storm, drifts between 1–6 km/day were about equally probable. Larger values were observed after the storm when the swell reached the oil-spill area—Stokes drift between 4 to 10 km/day became (roughly) equally likely. These values are consistent with global observations (e.g. Liu et al., 2014). There is evidence that Stokes drift can contribute significantly to the deflection angle of Ekman currents (Lewis and Belcher, 2004). Curcic et al. (2016) present unique numerical and observational evidence that during hurricane Isaac in 2012, Stokes drift contributed to about 20% of the Lagrangian flow magnitude (up to about 20 cm/s) and caused up to 20° in directional change. They also report increased submesoscale activity after the hurricane, suggesting increased diffusivity persists following extreme wind events.

Small-scales processes like waves breaking or Langmuir circulation can change the vertical position of particles considerably. However, it is LT that can significantly increase the submergence of buoyant particles in the ocean surface boundary layer (Kukulka and Brunner, 2015; Brunner et al., 2015). A recent study suggests that the effect of a vertical velocity in the upper mixed layer of the ocean could change the horizontal dispersion of particles dramatically (Aharon et al., 2012); this study was in the context of weak vertical advection associated with the diurnal cycle of heating and cooling. Döös et al. (2011) found that simulated trajectories with a vertical component increased their relative dispersion by 15%, as compared to the same trajectory simulation when constrained to a fixed-depth surface. In the context of oil-spill modeling, it has been known for some time that Langmuir circulation can be of importance (e.g. Simecek-Beatty and Lehr, 2000).

Another example of a small-scale process affecting trajectories near the ocean's surface that is not included in ocean-models is windage or leeway drift: the effect of wind acting directly on the passive object moving at the surface (e.g. Hackett et al., 2006); this is additional to the Ekman dynamics described above. Lehr and Simecek-Beatty (2000) suggest using 1–6% of the wind speed for wind drift.

These small-scale processes are often not represented in ocean models, even though there are parameterizations that are able to account for them (e.g. McWilliams et al., 2012). Indeed, Le Henaff et al. (2012) showed that adding a parameterization for the combined effect of Stokes drift, Langmuir circulation and waves breaking improved Deepwater Horizon (DWH) oil-spill simulations with HyCOM—an ocean model used by the U.S. Navy for prediction in the GoM. They found that the location of oil at sea and of landfall was improved, likewise the amount of oil beaching was more accurate when including the combined effect of these processes. It was the additional effect of wind drift that impeded the oil from entrainment into the loop current, thus improving the realism of their oil-spill simulation. Further description on the role of currents and wind during the DWH event can be found in Goni et al. (2015).

As understanding of the upper layer dynamics is improved, it becomes clear that trajectories near the ocean surface are highly dependent on local conditions, highlighting the need for observations; indeed, very fine observations may be needed. Röhrs and Christensen (2015) compared undrogued, specially-designed drifters at the sea surface and at 64 cm depth. The mean drift speed was 32 cm/s and 22 cm/s, respectively. The mean Stokes drift was 8.9 cm/s at the surface and 3.7cm/s at 64 cm depth. The magnitude of the drifter velocity at the surface (when windage is included) was 2.3% of the wind magnitude, and 1.3% at 64 cm deep. Deflection angles of the drifter velocity with respect to the wind were 73° and 62°, respectively. The smaller deflection angle right below the surface (64-cm depth) relative to the deflection at the surface is

consistent with deflection due to Stokes drift. These experiments show that substantial dynamical differences can happen within the first meter of the ocean. Other studies in different regions (referenced in the same paper), but using the same type of drifters reported reduced deflection angles both at the surface and right below the surface; this is likely due to local stratification conditions.

3.3 ON THE APPLICABILITY OF THE EKMAN-MADSEN SOLUTION AND ITS RELATION TO OTHER PHYSICAL PROCESSES

Often the upper ocean is observed to behave as a slab—velocity, temperature and salinity are vertically constant in the mixed layer. Beneath this layer they often have a strong vertical gradient. Models that simulate this behavior—bulk mixed-layer models—are often successful in reproducing observations. Rudnick (2001) suggests that the Ekman spiral and the bulk mixed-layer representation can be reconciled by noting that instantaneous observations are in good agreement with the mixed-layer model while temporal averages—especially if they include several cycles of daily surface heating and cooling—show an Ekman spiral (e.g. Stacey et al., 1986). This may seem at odds with the relatively short spin-up time of the Madsen model mentioned above. Discrepancies between the model and observations, however, should not be surprising given the simplifications implicit in Ekman theory, and that are necessary to isolate the fundamental turbulent effect of wind on the ocean's surface. For example, stratification is not represented in the Madsen or Ekman models, while it is known to be important and especially relevant for the time-dependence of the spiral in regions with a diurnal cycle of heating and cooling; nor is the wind's temporal variability taken into consideration although it could, and has been shown, to be important (e.g. Price et al., 1986). Likewise, the effect of waves and the density distribution (e.g. fronts) can be important (e.g. Wenegrat and McPhaden, 2016) and are not considered in the Madsen or Ekman models.

Nonetheless, deflection in the surface current relative to the wind direction is a robust response ubiquitously observed in the ocean and in numerical models. Even when the upper ocean behaves like a slab there is deflection, although there is no vertical dependence within the mixed layer. McNally and White (1985), for example, report a deflection angle of 17° for drifters drogued within a mixed layer. They find that this deflection angle includes windage and some unidentified process, and that the deflection angle due to slab-model Ekman dynamics is 30°; they cite other studies with the same deflection. The actual deflection is what concerns the problem of oil-spill simulations, therefore even with a successful slab-type Ekman model, the angle could be off due to missing physics. Furthermore, the analytic solution for the angle of deflection due to Ekman dynamics is very sensitive to the type of eddy diffusivity, to waves and to the stratification of the water column.

Overall the Madsen solution compares favorably with observations, suggesting an improvement over Ekman's original formulation (see e.g. Cushman-Roisin and Beckers, 2011). It is noted however, that significant variations should be expected depending on local conditions (e.g. references in Röhrs and Christensen, 2015). The example by McNally and White (1985) is important because it stresses that disentangling the dynamics may be difficult, that physics not typically included in ocean models can affect the angle of deflection and that the actual deflection angle varies considerably with local conditions (e.g. see their Table 3). An oil-spill model by Samuels et al. (1982) suggests using a varying angle updated at each time step because of these difficulties: "[f]ield and laboratory data suggest … that the deflection angle of the

surface drift current can be highly variable". They modulate the angle of deflection according to a seasonal dependence they base on data. However, they only seem to consider the seasonal variation of wind speed; it is not clear if they contemplate the effects of stratification which since then has been found to be important for the deflection of the ocean current relative to wind (e.g. Price et al., 1986; Heinloo and Toompuu, 2011; Wenegrat and McPhaden, 2016).

Another aspect specific to oil spills (e.g. Wu, 1983) is that when there is an oil slick at the surface, the wind-induced drift current is reduced as the wind-stress coefficient is reduced; however, this effect is somewhat compensated by an increase in wave-induced mass transport due to increased wave damping; this paper also discussed linear superposition of drifts.

Regarding the magnitude of wind drift, oil-spill modeling has typically used a 3% rule to determine the magnitude of the ocean current with respect to the magnitude of the wind. However, there should be some flexibility in choosing this parameter. To quote Lehr and Simecek-Beatty (2000):

> *Observational data indicates the wind drift factor can actually vary from 1% to 6%.*

Csanady (1997) uses an analytical model incorporating the effect of waves, Stokes drift and buoyancy fluxes to find that the surface velocity is about "3% of wind speed, varying within a range of about 2 to 4.5%". Note that this model does not incorporate Langmuir circulation that, according to Lehr and Simecek-Beatty (2000), can account by itself for a surface current as fast as 5.5% of the wind speed, albeit for a relatively short time period.

Likewise, Wu (1975) found that the wind-induced shear current plus wave-induced mass transport was 3–5% of the wind at long wave fetch, and he noted that the more commonly accepted value of 3% "is believed to be obtained with surface floats of appreciable sizes … such floats generally indicate a smaller drift".

If windage is negligible and if the ocean-model represents Ekman dynamics properly, then adding some percentage of the wind could be excessive, similar to adding the same quantity twice. Again, there is a need to assess each case individually.

3.3.1 User-Added Angle of Deflection and Speed

Given the wide range of variability found in observations and the difficulty of replicating the local dynamics responsible for the angle of deflection, it is natural to have an option in BLOSOM that would allow the user to input a deflection angle and a windage ocean-current speed as a percentage of the wind speed. This option is useful when additional in situ information is available or, in general, when an assessment can be made that the ocean model needs to be complemented. This option could also be useful even when using currents from HF radar (Abascal et al., 2012). The technical report by Allen and Plourde (1999) includes a vast amount of information on windage.

4. USING OBSERVATIONS INSTEAD OF OCEAN-MODELS

New ocean-current products based on observations instead of numerical simulations are being developed and made available. While it is likely that operational oil-spill forecasting will become strongly dependent on these products, it is important to keep in mind that the ability to observe the ocean is limited. Indeed, the following description applies to surface currents only. Ocean models will therefore remain a necessary tool, extending observations not only below the sea surface, but also horizontally to regions where observations are scarce or not available. Blending observations with ocean models is standard procedure for operational models. The blending happens routinely through data assimilation; however, alternative approaches where only the velocity field is corrected by using drifter data have been shown to improve results (e.g. Toner et al., 2001, more examples below).

The following is an example of an ocean-current product derived from observations; this example continues to stress the variability of near-surface dynamics. Other promising examples of ocean-current products follow.

Rio et al. (2014) combine improved geostrophic currents from remote sensing (satellite altimetry) with an empirical model for the Ekman velocity to produce 3-hourly, global-ocean currents at the surface and at 15-m depth from 1993 to 2013. There are two improvements to the geostrophic currents in this product relative to prior estimates. The first one is due to a better geoid model (Gravity and Ocean Circulation Experiment) resulting in a more accurate mean dynamic topography; the sea level anomaly is thus better complemented. This results in an absolute dynamic topography accurate to the centimeter at horizontal scales of 100–150 km.

The second improvement incorporates in situ measurements to recover smaller-scale currents not available in the altimetry-derived large-scale measurements. To this purpose they first construct an Ekman model from the reanalysis (ERA-Interim reanalysis) of an atmospheric forecast model that incorporates observations (including satellite-derived wind). The Ekman model itself is a useful byproduct that can be used for spatially- and temporally-varying estimation of Ekman currents at the surface and at 15-m depth. Two parameters are estimated, one of them is the angle of deflection relative to the wind. Rio et al. (2014) find that monthly-mean deflections at the surface in the Northern Hemisphere vary between a minimum of 25° in the boreal winter to a maximum of about 38° in July and August (boreal summer). A similar temporal behavior is observed at 15-m depth, but with values of 45° and 62° for winter and summer, respectively. The southern hemisphere has maximum deflection values during the austral summer of about 29° (surface) and 57° (at 15 m), and a minimum deflection during austral winter (July and August) of 23° and 43°. These results are consistent with the effect of stratification. Indeed, stratification is essential for accurate estimations of the amount of wind energy entering the ocean's surface layer (e.g. Kilbourne and Girton, 2015). Other similar sea-surface velocity products are available (e.g. Sudre et al., 2013).

The concept of extracting small-scale information using drifters can be extended to (almost) real-time currents if drifters are promptly deployed to the region of interest. Berta et al. (2015) show that, in the GoM, geostrophic currents from altimetry may be adequate for Lagrangian transport despite the coarse resolution, and that complementing this information with drifters dramatically improves the quality of simulated trajectories. However, each region should be considered separately: there is growing evidence that in the GoM it is the mesoscale circulation that drives

particle dispersion, and that motion at scales of 50 km and greater could be enough to predict Lagrangian motion (see references in the introduction) yet, this may not always be the case.

It is nevertheless encouraging that by including drifters a considerable improvement results in the estimated circulation near De Soto canyon and over the shelf—regions where smaller-scale structures are predominant (Berta et al., 2015; they also show that the amount of drifters needed for their methodology is affordable).

High-frequency radar (HF radar) is a remote sensing system able to measure sea-surface currents with good accuracy over coastal areas (Paduan and Washburn, 2013; Rypina et al., 2014); it is increasingly available in the U.S. (e.g. http://hfradar.ndbc.noaa.gov/) and around the world.

Using HF radar currents to track pollutants is promising because of the availability of real-time, long-term accurate measurements with relatively high spatial and temporal resolutions (e.g. Frolov et al., 2012). Typical error estimates in trajectories computed from HF radar currents are 7–10 km per day (Ullman et al., 2006), however recent improvements in data processing of HF radar data (Kirincich et al., 2012) resulted in trajectory error estimates of 3–4 km per day (Rypina et al., 2014).

HF radar can be rapidly deployed to a region where no measurements are available in the event of an oil-spill (Barrick et al., 2012). Depending on the resolution and the local physics however, HF radar measurements may still need complementing with information on the small-scale processes as shown by Rypina et al. (2014). They further point out that for long-term trajectory estimation, a regional ocean model that assimilates the HF radar currents might be necessary.

Berta et al. (2014) show that when drifters are promptly deployed, trajectories computed from HF radar or ocean models can be significantly improved, reducing error estimates from 6 km trajectory-separation per day to 2 km per day (this also requires deploying the drifters in the right places). They show that with their methodology there is some forecasting skill for about 6-hr periods.

Diffusivity can be computed from ocean-model trajectories and then compared to the diffusivity from drifter observations at sea, thus missing physics can be evaluated and parametrized. De Dominicis et al. (2012) suggest that with high-frequency sampling (enough to resolve fluctuations happening within an hour) it could be possible to estimate the LTS and diffusivity for Lagrangian particles. However, the above approach by Berta et al. (2014 and 2015) seems a better solution since it also corrects the large-scale velocity.

Other methods to measure surface ocean currents with high resolution are being developed and seem promising, e.g. the use of airborne radar (Martin et al., 2016).

5. OUTLOOK

Oil-spill models should be able to complement ocean-model velocity with additional parameterizations. Ideally ocean-current velocity, should be fine-tuned with observations at the location and time of interest. The ability to incorporate observations and simulations, and to flexibly blend whatever may be available to produce accurate ocean currents is likely to become the future of oil-spill modeling. This strategy should therefore guide the development map for BLOSOM.

There should be an option to add additional physics when observations are not available; at the time this report was developed, BLOSOM uses Madsen's model to include the effect of wind. Some more advanced algorithms may be tested and added to BLOSOM in future releases. Suggestions include:

- A recent Ekman model including the effect of stratification and Stokes drift compared favorably with observations suggesting an improvement with respect to Ekman's original model (Heinloo and Toompuu, 2011). Another similar model is by Wenegrat and McPhaden (2016).
- Methods to project surface observations into the water column are making encouraging progress (e.g. LaCasce and Wang, 2015) and will perhaps become an important part of a solution to replicating ocean currents accurately. Furthermore, it is conceivable that the Ekman models that include stratification could benefit from the stratification projection methods that LaCasce and Wang (2015) use.
- Le Henaff et al. (2012) give equations to compute Stokes drift, the effect of Langmuir circulations and waves breaking directly from winds (ideally the same winds forcing the ocean model should be used for consistency; see their supplemental information). Wu et al. (2015) also include a method to compute Stokes drift directly from a two-dimensional wave spectrum.

6. CONCLUSION.

There are two approaches to oceanic oil-spill modeling, and both approaches are useful. The first involves hindcasting or forecasting a specific oil-spill, this requires accurate information of all the relevant physics. The second approach is probabilistic: a large number of simulations with different conditions are run and probabilities are computed from the results. In this case, the processes affecting trajectories can be varied to create a simulation ensemble.

By looking at several examples, this report demonstrated that the ocean's response is a complex and diverse combination of factors, making it difficult to simulate any particular event precisely. This is true at small and large scales although the large-scale processes often have a greater effect. This report focused on the small-scale processes. One implication is that observations are critical for both the development and assessment of oil-spill modeling.

On-going oceanographic research will likely result in: 1) better parameterizations that allow incorporation of small-scale processes when necessary, 2) increasingly accurate sea-surface velocity products, and 3) the continuing improvement of numerical ocean models and the data assimilation they use. Any modern oil-spill model should be able to tread all of these waters successfully; synergistic approaches will likely remain critical for the difficult problem of simulating accurate trajectories in the ocean's currents.

Oil-spill modelers should be qualified to assess the importance of the different processes affecting the accuracy of simulations, and to leverage the tools made available to remediate potential problems.

7. REFERENCES.

Abascal, A. J.; Castanedo, S.; Fernández, V.; Medina, R. Backtracking drifting objects using surface currents from high-frequency (HF) radar technology. *Ocean Dynamics* **2012,** *62*, 1073–1089.

Aharon R.; Rom-Kedar, V.; Gildor, H. When complexity leads to simplicity: Ocean surface mixing simplified by vertical convection. *Physics of Fluids* **2012,** *24*, 056603.

Alexanderian, A.; Winokur, J.; Sraj, I.; Srinivasan, A.; Iskandarani, M.; Thacker, W. C.; Knio, O. M. Global sensitivity analysis in an ocean general circulation model: A sparse spectral projection approach. *Computational Geosciences* **2012,** *16*, 757–778. http://doi.org/10.1007/s10596-012-9286-2

Allen, A. A.; Plourde, J. V. *Review of Leeway: Field Experiments and Implementation*; U.S. Coast Guard Research and Development Center, 1999.

Barrick, D.; Fernandez, V.; Ferrer, M. I.; Whelan, C.; Breivik, Ø. A short-term predictive system for surface currents from a rapidly deployed coastal HF radar network. *Ocean Dynamics* **2012,** *62*, 725–740.

Bauer, S.; Swenson, M. S.; Griffa, A. Eddy mean flow decomposition and eddy diffusivity estimates in the tropical Pacific Ocean: 2. Results. *Journal of Geophysical Research* **2002,** *107*, 3154. DOI:10.1029/2000JC000613

Beron-Vera, F. J.; LaCasce, J. H. Statistics of simulated and observed pair separations in the Gulf of Mexico. *Journal of Physical Oceanography* **2016,** in press.

Beron-Vera, F. J.; Olascoaga, M. J. An Assessment of the Importance of Chaotic Stirring and Turbulent Mixing on the West Florida Shelf. *J. Phys. Oceanogr.* **2009,** *39*, 1743–1755. DOI:10.1175/2009JPO4046.1. http://journals.ametsoc.org/doi/abs/10.1175/2009JPO4046.1

Berta, M.; Bellomo, L.; Magaldi, M. G. Estimating Lagrangian transport blending drifters with HF radar data and models: results from the TOSCA experiment in the Ligurian Current (North Western Mediterranean Sea). *Progress in Oceanography* **2014,** *0*, 15–29. http://doi.org/10.1016/j.pocean.2014.08.004

Berta, M.; Griffa, A.; Magaldi, M. G.; Özgökmen, T. M.; Poje, A. C.; Haza, A. C.; Olascoaga, M. J. Improved Surface Velocity and Trajectory Estimates in the Gulf of Mexico from Blended Satellite Altimetry and Drifter Data. *Journal of Atmospheric and Oceanic Technology* **2015,** *32*, 1880–1901. http://doi.org/10.1175/JTECH-D-14-00226.1

Brunner, K.; Kukulka, T.; Proskurowski, G.; Law, K. L. Passive buoyant tracers in the ocean surface boundary layer: 2. Observations and simulations of microplastic marine debris. *J. Geophys. Res. Oceans* **2015,** *120*, 7559–7573. DOI:10.1002/2015JC010840.

Callies, J.; Ferrari, R.; Klymak, J. M.; Gula, J. Seasonality in submesoscale turbulence. *Nature Communications* **2015,** *6*, 6862. DOI: 10.1038/ncomms7862

Chassignet, E. P.; Verron, J. Ocean Modeling and Parameterization; NATO Science Series; Springer, 1998.

Chiswell, S. M. Lagrangian timescales and eddy diffusivity at 1000 m compared to the surface in the south Pacific and Indian Oceans. *J. Phys. Oceanogr.* **2013,** 130920111559006. DOI:10.1175/JPO-D-13-044.1. http://journals.ametsoc.org/doi/abs/10.1175/JPO-D-13-044.1

Clark, M. Quantification of Stokes Drift as a Mechanism for Surface Oil Advection in the Gulf of Mexico during the Deepwater Horizon Oil Spill. Electronic Theses, Florida State University, Treatises and Dissertations, 2015; Paper 9576.

Csanady, G. T. Circulation in the Coastal Ocean. Reidel Publishing, 1982.

Csanady, G. T. The "Slip Law" of the Free Surface. *Journal of Oceanography* **1997,** *53*, 67–80.

Curcic, M.; Chen, S. S.; Özgökmen, T. M. Hurricane-Induced Ocean Waves and Stokes Drift and their Impacts on Surface Transport and Dispersion in the Gulf of Mexico. *Geophysical Research Letters* **2016,** *43*, 2773–2781. http://doi.org/10.1002/2015GL067619

Cushman-Roisin, B.; Beckers, J. *Introduction to Geophysical Fluid Dynamics: Physical and Numerical Aspects*; Elsevier, 2011.

D'Asaro, E. Turbulence in the Upper-Ocean Mixed Layer. *Annu. Rev. Mar. Sci.* **2014,** *6*, 101–15.

De Dominicis, M.; Leuzzi, G.; Monti, P.; Pinardi, N.; Poulain, P.-M. Eddy diffusivity derived from drifter data for dispersion model applications. *Ocean Dynamics* **2012,** *62*, 1381–1398. http://doi.org/10.1007/s10236-012-0564-2

Döös, K.; Rupolo, V.; Brodeau, L. Dispersion of surface drifters and model-simulated trajectories. *Ocean Model* **2011,** *39*, 301–310.

Durski, S. M.; Glenn, S. M.; Haidvogel, D. B. Vertical mixing schemes in the coastal ocean: Comparison of the level 2.5 Mellor-Yamada scheme with an enhanced version of the K profile parameterization. *J. Geophys. Res.* **2004,** *109*, C01015. DOI:10.1029/2002JC001702

Ferrari, R.; Wunsch, C. Ocean Circulation Kinetic Energy: Reservoirs, Sources, and Sinks. *Annu. Rev. Fluid Mech.* **2009,** *41*, 253–82

Fischer, H. B.; List, E. J.; Hoh, R. C.Y.; Imberger, J.; Brooks, N. H. *Mixing in inland and coastal waters*, 2nd Ed.; Academic Press, 1979.

Frolov S.; Paduan, J.; Cook, M.; Bellingham, J. Improved statistical prediction of surface currents based on historic HF-radar observations. *Ocean Dynamics* **2012,** *62*, 1111–1122.

Gent P. R. The Gent-McWilliams paramterization: 20/20 hindsight. *Ocean Modelling* **2011,** *39*, 2–9.

Gillespie, D. Exact numerical simulation of the Ornstein-Uhlenbeck process and its integral. *Physical Review E* **1996,** *54*, 2084–2091. http://doi.org/10.1103/PhysRevE.54.2084

Goni, G. J.; Trinanes, J. A.; MacFadyen, A.; Streett, D.; Olascoaga, M. J.; Imhoff, M. L.; Muller-Karger, F.; Roffer, M. A. Variability of the Deepwater Horizon Surface Oil Spill Extent and Its Relationship to Varying Ocean Currents and Extreme Weather Conditions. Chapter in *Mathematical Modelling and Numerical Simulation of Oil Pollution Problems*; Ehrhardt, M., Ed.; Springer: 2015.

Griffa, A.; Piterbarg, L. I.; Özgökmen, T. Predictability of Lagrangian particle trajectories: Effects of smoothing of the underlying Eulerian flow. *J. Mar. Res.* **2004,** *62*, 1–35.

Griffies, S. M. *Fundamentals of Ocean Climate Models*; Princeton University Press, 2004.

Hackett, B.; Breivik, Ø.; Wettre, C. Forecasting the Drift of Objects and Substances in the Ocean. In *Ocean Weather Forecasting*; Chassignet, E. P., Verron J., Eds.; Springer, 2006.

Haza, A. C.; Özgökmen, T. M.; Griffa, A.; Garraffo, Z. D.; Piterbarg, L. Parameterization of particle transport at submesoscales in the Gulf Stream region using Lagrangian subgridscale models. *Ocean Model* **2012,** *42*, 31–49. DOI:10.1016/j.ocemod.2011.11.005. http://dx.doi.org/10.1016/j.ocemod.2011.11.005.

Haza, A. C.; Poje, A. C.; Özgökmen, T. M.; Martin, P. Relative dispersion from a high-resolution coastal model of the Adriatic Sea. *Ocean Modelling* **2008,** *22*, 48–65. http://doi.org/10.1016/j.ocemod.2008.01.006

Heemink, A. W. Stochastic modelling of dispersion in shallow water. *Stoch. Hydrol. Hydraul.* **1990,** *4*, 161–174. DOI:10.1007/BF01543289.

Hunter, J. R.; Craig, P. D.; Phillips, H. E. On the use of random walk models with spatially variable diffusivity. *Journal of Computational Physics* **1993,** *106*, 366–376. http://doi.org/10.1016/S0021-9991(83)71114-9

Jacobs, G. A.; Huntley, H. S.; Kirwan, A. D.; Lipphardt, B. L.; Campbell, T.; Smith, T.; Edwards, K.; Bartels, B. Ocean processes underlying surface clustering. *J. Geophys. Res. Oceans* **2016,** *121*, 180–197. DOI:10.1002/2015JC011140.

Kackett, B.; Breivik, O.; Wettre, C. Forecasting the Drift of Objects and Substances in the Ocean, Chapter 23. In *Ocean Weather Forecasting*; Chassignet, E. P., Verron, J., Eds. Springer, 2006; p 507–523.

Keating, S. R.; Smith, K. S.; Kramer, P. R. Diagnosing Lateral Mixing in the Upper Ocean with Virtual Tracers: Spatial and Temporal Resolution Dependence. *Journal of Physical Oceanography* **2011,** *41*, 1512–1534. http://doi.org/10.1175/2011JPO4580.1

Kilbourne, B. F.; Girton, J. B. Surface boundary layer evolution and near-inertial wind power input. *J. Geophys. Res. Oceans* **2015,** *120*, 7506–7520. DOI:10.1002/2015JC011213.

Klein, P.; Lapeyre, G. The Oceanic Vertical Pump Induced by Mesoscale and Submesoscale Turbulence. *Annu. Rev. Mar. Sci.* **2009,** *1*, 351–75.

Kraus, E. B.; Businger, J. A. *Atmosphere-Ocean Interaction*, 2nd ed.; Oxford University Press, 1994.

Kukulka, T.; Brunner, K. Passive buoyant tracers in the ocean surface boundary layer: 1. Influence of equilibrium wind-waves on vertical distributions. *J. Geophys. Res. Oceans* **2015,** *120*, 3837–3858. DOI:10.1002/ 2014JC010487.

LaCasce, J. H. Statistics from Lagrangian observations. *Prog. Oceanogr.* **2008,** *77*, 1–29. DOI:10.1016/j.pocean.2008.02.002.

Lacorata, G.; Palatella, L.; Santoleri, R. Lagrangian predictability characteristics of an Ocean Model. *J. Geophys. Res. Oceans* **2014,** *119*, 8029–8038. DOI:10.1002/ 2014JC010313.

Large W. G.; McWilliams J. C.; Doney, S. C. Oceanic Vertical Mixing: A Review and A Model With a Nonlocal Boundary Layer Parameterization. *Reviews of Geophysics* **1994,** *32*, 363–403.

Le Henaff, M.; Kourafalou, V. H.; Paris, C. B.; Helgers, J.; Aman, Z. M.; Hogan, P. J.; Srinivasan, A. Surface Evolution of the Deepwater Horizon Oil Spill Patch: Combined Effects of Circulation and Wind-Induced Drift. *Environ. Sci. Technol.* **2012,** *46*, 7267–7273.

Ledwell, J. R.; He, R.; Xue, Z.; DiMarco, S. F.; Spencer, L.; Chapman, P. Dispersion of a tracer in the deep Gulf of Mexico. *J. Geophys. Res. Ocean.* **2016**. DOI:10.1002/2015JC011405. http://doi.wiley.com/10.1002/2015JC011405

Lehr, J. W.; Simecek-Beatty, D. The Relation of Langmuir Circulation Processes to the Standard Oil Spill Spreading, Dispersion, and Transport Algorithms. *Spill Science & Technology Bulletin* **2000,** *6*, 247–253. http://doi.org/10.1016/S1353-2561(01)00043-3

Lentz, S. J. The Surface Boundary Layer in Coastal Upwelling Regions. *J. Phys. Oceanogr.* **1992,** *22*, 1517–1539.

Lewis, D. M.; Belcher, S. E. Time-dependent, coupled, Ekman boundary layer solutions incorporating Stokes drift. *Dynamics of Atmospheres and Oceans* **2004,** *37*, 313–351. http://doi.org/10.1016/j.dynatmoce.2003.11.001

Liu, G.; Perrie, W. A.; He, Y. Ocean surface Stokes drift from scatterometer observations. *International Journal of Remote Sensing* **2014,** *35*, 1966–1978. DOI: 10.1080/01431161.2014.880818

Liu, Y.; Weisberg, R. H.; Vignudelli, S.; Mitchum, G. T. Evaluation of altimetry-derived surface current products using Lagrangian drifter trajectories in the eastern Gulf of Mexico. *J. Geophys. Res. Ocean* **2014,** 7772–7793. DOI:10.1002/2014JC010019.

Lumpkin, R.; Treguier, A.-M.; Speer, K. Lagrangian Eddy Scales in the Northern Atlantic Ocean. *Journal of Physical Oceanography* **2002,** *32*, 2425–2440. http://doi.org/10.1175/1520-0485-32.9.2425

Madsen, O. S. A Realistic Model of the Wind-Induced Ekman Boundary Layer. *Journal of Physical Oceanography* **1977,** *7*, 248–255.

Martin, A. C. H.; Gommenginger, C.; Marquez, J.; Doody, S.; Navarro, V.; Buck, C. Wind-Wave induced velocity in ATI SAR Ocean Surface Currents: First experimental evidence from an airborne campaign. *Journal of Geophysical Research: Oceans* **2016,** *121*, 1640–1653. http://doi.org/10.1002/2015JC011459

Maurizi, A.; Griffa, A.; Poulain, P.-M.; Tampieri, F. Lagrangian turbulence in the Adriatic Sea as computed from drifter data: Effects of inhomogeneity and nonstationarity. *J. Geophys. Res.* **2004,** *109*, C04010. DOI:10.1029/2003JC002119. http://doi.wiley.com/10.1029/2003JC002119

McNally, G. J.; White, B. Wind driven flow in the mixed layer observed by drifting buoys during autumn-winter in the midlatitude North Pacific. *Journal of Physical Oceanography* **1985,** *15*, 684–694.

McNutt, M. K.; Camilli, R.; Crone, T. J.; Guthrie, G. D.; Hsieh, P. A.; Ryerson, T. B.; Savas, O.; Shaffer, F. Review of flow rate estimates of the Deepwater Horizon oil spill. *Proc. Natl. Acad. Sci.* **2012,** *109*, 20260–20267. DOI:10.1073/pnas.1112139108. http://www.pnas.org/content/109/50/20260.abstract

McWilliams, J. C.; Huckle E.; Liang, J.-H.; Sullivan, P. P. The Wavy Ekman Layer: Langmuir Circulations, Breaking Waves, and Reynolds Stress. *J. Phys. Oceanogr.* **2012,** *42*, 1793–1816. DOI: http://dx.doi.org/10.1175/JPO-D-12-07.1

McWilliams, J. C.; Restrepo J.M. The Wave-Driven Ocean Circulation. *J. Phys. Oceanogr.* **1999,** *29*, 2523–2540.

Middleton, J. F. Drifter spectra and diffusivities. *Journal of Marine Research* **1985,** *43*, 37–55.

Moum, J. N.; Rippeth, T. P. Do observations adequately resolve the natural variability of oceanic turbulence? *Journal of Marine Systems* **2009,** *77*, 409–417. http://doi.org/10.1016/j.jmarsys.2008.10.013

Moum, J. N.; Smyth, W.D. Upper Ocean Mixing Processes. A derivative of *Encyclopedia of Ocean Sciences, Elements of Physical Oceanography*; 2nd ed.; Academic Press, 2001; p 281–287.

Müller P.; von Storch, H. *Computer Modelling in Atmospheric and Oceanic Sciences*; Springer, 2004.

Muller-Karger, F. E.; Smith, J. P.; Werner, S.; Chen, R.; Roffer, M.; Liu, Y.; Enfield, D. B. Natural variability of surface oceanographic conditions in the offshore Gulf of Mexico. *Progress in Oceanography* **2015,** *134*, 54–76. http://doi.org/10.1016/j.pocean.2014.12.007

Olascoaga, M. J.; Beron-Vera, F. J.; Haller, G.; Trinanes, J.; Iskandarani, M.; Coelho, E. F.; Haus, B. K.; Huntley, H. S.; Jacobs, G.; Kirwan, Jr., A. D.; Lipphardt, Jr., B. L.; Ozgokmen, T. M.; Reniers, A. J. H. M.; Valle-Levinson, A. Drifter motion in the Gulf of Mexico constrained by altimetric Lagrangian coherent structures. Geophys. Res. Lett. **2013,** *40*, 6171–6175. DOI:10.1002/2013GL058624. http://doi.wiley.com/10.1002/2013GL058624

Paduan J. D.; Washburn, L. High-Frequency Radar Observations of Ocean Surface Currents. *Annual Review of Marine Science* **2013,** *5*, 115–36. DOI: 10.1146/annurev-marine-121211-172315.

Poje, A. C.; Haza, A. C.; Özgökmen, T. M.; Magaldi, M. G.; Garraffo, Z. D. Resolution dependent relative dispersion statistics in a hierarchy of ocean models. *Ocean Modelling* **2010,** *31*, 36–50. http://doi.org/10.1016/j.ocemod.2009.09.002

Price, J. F.; Weller, R. A.; Pinkel, R. Diurnal cycling: Observations and models of the upper ocean response to diurnal heating, cooling, and wind mixing. *Journal of Geophysical Research* **1986,** *91*, 8411. http://doi.org/10.1029/JC091iC07p08411

Qiu, B.; Chen, S.; Klein, P.; Sasaki, H.; Sasai, Y. Seasonal Mesoscale and Submesoscale Eddy Variability along the North Pacific Subtropical Countercurrent. *Journal of Physical Oceanography* **2014,** *44*. DOI: 10.1175/JPO-D-14-0071.1

Rio, M.; Mulet, S.; Picot, N. Beyond GOCE for the ocean circulation estimate: Synergetic use of altimetry, gravimetry, and in situ data provides new insight into geostrophic and Ekman current. *Geophysical Research Letters* **2014,** *41*, 8918–8925. http://doi.org/10.1002/2014GL061773

Röhrs, J.; Christensen, K. H. Drift in the uppermost part of the ocean. *Geophysical Research Letters* **2015,** 1–8. http://doi.org/10.1002/2015GL066733.1

Rudnick, D. L. (2001). Upper ocean space and time variability in Elements of Physical Oceanography: A derivative of the Encyclopedia of Ocean Sciences 2nd Edition, 2009.

Rupolo, V. A Lagrangian-Based Approach for Determining Trajectories Taxonomy and Turbulence Regimes. *Journal of Physical Oceanography* **2007a**. http://doi.org/10.1175/JPO3038.1

Rupolo, V. Observing Turbulence Regimes and Lagrangian Dispersal Properties in the Ocean. In *Lagrangian Analysis and Prediction of Coastal and Ocean Dynamics*; Griffa, A., Kirwan, Jr., A. D., Mariano, A. J., Özgökmen, T., Rossby, H. T., Cambridge University Press, 2007b.

Rypina I. I.; Kirincich, A. R.; Limeburner, R.; Udovydchenkov, I. A. Eulerian and Lagrangian Correspondence of High-Frequency Radar and Surface Drifter Data: Effects of Radar Resolution and Flow Components. *J. Atmos. Oceanic Technol.* **2014,** *31*, 945–966.

Sallée, J. B.; Speer, K.; Morrow, R.; Lumpkin, R. An estimate of Lagrangian eddy statistics and diffusion in the mixed layer of the Southern Ocean. *Journal of Marine Research* **2008,** *66*, 441–463.

Samelson, R. M. Coastal Boundary Conditions and the Baroclinic Structure of Wind-Driven Continental Shelf Currents. *J. Phys. Oceanogr.* **1997,** *27*, 2645–2662. DOI: http://dx.doi.org/10.1175/1520-0485(1997)027<2645:CBCATB>2.0.CO;2

Samuels, W. B.; Huang, N. E.; Amstutz, D. E. An oilspill trajectory analysis model with a variable wind deflection angle. *Ocean Engineering* **1982,** *9*, 347–360. http://doi.org/10.1016/0029-8018(82)90028-2

Shcherbina, A. Y.; Sundermeyer, M. A.; Kunze, E.; D'Asaro, E.; Badin, G.; Birch, D.; Ledwell, J. R. The latmix summer campaign: Submesoscale stirring in the upper ocean. *Bulletin of the American Meteorological Society* **2015,** *96*, 1257–1279. http://doi.org/10.1175/BAMS-D-14-00015.1

Sim, L.; Graham, J.; Rose, K.; Duran, R.; Nelson, J.; Umhoefer, J.; Vielma, J. *Developing a Comprehensive Deepwater Blowout and Spill Model*; NETL-TRS-9-2015; EPAct Technical Report Series; U.S. Department of Energy, National Energy Technology Laboratory: Albany, OR, 2015; p 44.

Simecek-Beatty, D.; Lehr, W. J. Langmuir Circulation and Oil Spill Trajectory Models Workshop – Comments and Recommendations. *Spill Science & Technology Bulletin* **2000,** *6*, 273–274. http://doi.org/10.1016/S1353-2561(01)00046-9

Skyllingstad E. D.; Paluszkiewicz, T.; Denbo, D. W.; Smyth, W. D. Nonlinear vertical mixing processes in the ocean: modeling and paramterization. *Physica D: Nonlinear Phenomena* **1996,** *98*, 574–593.

Smagorinsky, J. Some historical remarks on the use of nonlinear viscosities. *Large Eddy Simulation of Complex Engineering and Geophysical Flows*; Galerpin, B., Orsag S. A., Eds.; Cambridge University Press, 1993; p 3–36.

Stacey, M. W.; Pond, S.; LeBlond, P. H. A wind-forced Ekman spiral as a good statistical fit to low-frequency currents in coastal strait. *Science* **1986,** *233*, 470–472.

Sudre, J.; Maes, C.; Garcon, V. On the global estimates of geostrophic and Ekman surface currents. *Limnology & Oceanography: Fluids & Environments* **2013,** *3*, 1–20. http://doi.org/10.1215/21573689-2071927

Tennekes, H.; Lumley, J. L. *A first course in turbulence*; The MIT Press, 1972.

Thorpe, S. A. *An introduction to ocean turbulence*; Cambridge University Press, 2007.

Toner, M.; Kirwan, A. D.; Kantha, L. H.; Choi, J. K. Can general circulation models be assessed and their output enhanced with drifter data? *J. Geophys. Res.* **2001,** *106*, 19563. DOI:10.1029/2000JC000587.

Ullman, D.; Codiga, D. Seasonal variation of a coastal jet in the Long Island Sound outflow region based on HF radar and Doppler current observations. *J. Geophys. Res.* **2004,** *109*, C07S06. DOI:10.1029/2002JC001660

Valentine, D. L.; Fisher, G. B.; Bagby, S. C.; Nelson, R. K.; Reddy, C. M.; Sylva, S. P.; Woo, M. A. Fallout plume of submerged oil from Deepwater Horizon. *Proc. Natl. Acad. Sci.* **2014,** *111*, 15906–15911. DOI:10.1073/pnas.1414873111. http://www.pnas.org/content/111/45/15906.abstract

Veronis, G. The role of models in tracer studies. In *Numerical Models of Ocean Circulation*; National Academy of Science, 1975.

Wenegrat, J. O.; McPhaden, M. J. Wind, Waves, and Fronts: Frictional Effects in a Generalized Ekman Model. *Journal of Physical Oceanography* **2016,** *46*, 371–394. http://doi.org/10.1175/JPO-D-15-0162.1

Wu, J. Sea-Surface Drift Currents Induced by Wind and Waves. *J. Phys. Oceanogr.* **1983,** *13*, 1441–1451. DOI:10.1175/1520-0485(1983)013<1441:SSDCIB>2.0.CO;2. http://dx.doi.org/10.1175/1520-0485(1983)013<1441:SSDCIB>2.0.CO

Wu, J. Wind-induced drift currents. *Journal of Fluid Mechanics* **1975,** *68*, 49–70.

Wu, L.; Rutgersson, A.; Sahlée, E. Upper-ocean mixing due to surface gravity waves. *J. Geophys. Res. Oceans* **2015,** *120*, 8210–8228. DOI:10.1002/2015JC011329.

Zhong, Y.; Bracco, A. Submesoscale impacts on horizontal and vertical transport in the Gulf of Mexico. *J. Geophys. Res. Ocean.* **2013,** *118*, 5651–5668. DOI:10.1002/jgrc.20402.

Sean Plasynski
Executive Director
Technology Development & Integration Center
National Energy Technology Laboratory
U.S. Department of Energy

John Wimer
Associate Director
Strategic Planning
Science & Technology Strategic Plans & Programs
National Energy Technology Laboratory
U.S. Department of Energy

Roy Long
Technology Manager
Science & Technology Strategic Plans & Programs
National Energy Technology Laboratory
U.S. Department of Energy

Elena Melchert
Director
Division of Upstream Oil and Gas Research
U.S. Department of Energy

Cynthia Powell
Executive Director
Research & Innovation Center
National Energy Technology Laboratory
U.S. Department of Energy